

Collective intersubband transitions in quantum wells: a comparative density-functional study

C. A. Ullrich and G. Vignale

Department of Physics, University of Missouri, Columbia, Missouri 65211

(August 13, 2018)

Abstract

We use linearized time-dependent (current) density functional theory to study collective transitions between the two lowest subbands in GaAs/AlGaAs quantum wells. We focus on two particular systems, for both of which experimental results are available: a wide single square well, and a narrow asymmetric double quantum well. The aim is to calculate the frequency and linewidth of collective electronic modes damped through electron-electron interaction only. Since Landau damping, i.e. creation of single electron-hole pairs, is not effective here, the dominant damping mechanism involves dynamical exchange-correlation effects such as multipair production. To capture these effects, one has to go beyond the widely used adiabatic local density approximation (ALDA) and include retardation effects. We perform a comparative study of two approaches which fall in this category. The first one is the dynamical extension of the ALDA by Gross and Kohn. The second one is a more recent approach which treats exchange and correlation beyond the ALDA as viscoelastic stresses in the electron liquid. It is found that the former method is more robust: it performs similarly for strongly different degrees of collectivity of the electronic motion. Results for single and double quantum wells compare reasonably to experiment, with a tendency towards overdamping. The viscoelastic approach, on the other hand, is superior for systems where the electron dynamics is predominantly collective, but breaks down if the local velocity field is too rapidly varying, which is the case for single-electron-like behavior such as tunneling through a potential barrier.

71.10.Ca;71.45Gm;73.20Dx,Mf;78.20.Ci;31.15.Ew

I. INTRODUCTION

In recent years, time-dependent density functional theory (TDDFT)^{1,2} has become the method of choice for describing dynamical electronic properties of atoms, molecules and solids in the linear regime and beyond. Until now, TDDFT has been mostly applied within the adiabatic local density approximation (ALDA)³ for the dynamical exchange-correlation (xc) potential. However, some propositions have been put forward for improving upon the ALDA. The objective of earlier attempts^{4,5} was to obtain approximations for the xc potential which would still be local in space, but not in time. All these approximations were found to suffer from inconsistencies, such as the failure to satisfy the so called “harmonic potential theorem” (HPT)⁵⁻⁷, and other basic symmetries. Only recently it has become clear that the root of these difficulties lies in the fact that the xc potential in TDDFT is an intrinsically nonlocal functional of the density, that is, a functional that does not admit an expansion in terms of the density gradients^{8,9}. Consequently, the most recent extensions of TDDFT beyond the ALDA are formulated in terms of the local *current* density¹⁰ or the motion of local fluid elements of the electron liquid¹¹.

Among the variety of phenomena which have been investigated using TDDFT methods (see Ref. 2 for a recent review), collective electronic excitations in semiconductor heterostructures are currently of great theoretical and experimental interest. In particular, much effort has gone into the study of parabolic quantum wells with and without imperfections¹²⁻¹⁶. However, the only collective mode that a uniform external field can excite in a parabolic well is the well-known center-of-mass mode⁷, which involves no internal compression of the electron gas. We therefore focus in this paper on the electronic response in single^{17,18} and double¹⁹⁻²³ square wells where no such restriction exists.

The need for going beyond the ALDA becomes evident if one is interested in the linewidth of these electronic excitations. The ALDA accounts for Landau damping of collective modes, i.e. decay into single particle-hole pairs²⁴. For high-frequency, long-wavelength modes, however, this decay mechanism is not effective, and damping is instead induced by *dynamical* xc effects such as multipair production. In other words, outside the regime where Landau damping occurs, the modes calculated within the ALDA will come out undamped. This limitation is overcome in non-adiabatic theories. In particular, in the formalism of Vignale, Ullrich and Conti (VUC)¹⁰, dynamical exchange and correlation lead to the appearance of viscoelastic stresses in the electron fluid, with complex and frequency-dependent viscosity coefficients depending on properties of the homogeneous electron gas. The viscosity causes an additional damping not contained in the ALDA.

In an earlier paper²⁵, the VUC formalism was used in a model system of two-dimensional quantum strips, where it predicts a substantial inhomogeneity-induced enhancement of the damping of collective modes compared to plasmons in the two-dimensional electron gas. The interest in this model system is based on two reasons: first of all, it is analytically solvable, and second, it satisfies the conditions of validity of the approach, namely $|\nabla n_0(\mathbf{r})|/n_0(\mathbf{r}) \ll k_F(\mathbf{r})$ and $\omega/v_F(\mathbf{r})$, where $n_0(\mathbf{r})$, $k_F(\mathbf{r})$ and $v_F(\mathbf{r})$ are the local equilibrium density, Fermi momentum and velocity. However, no experimental results are available to compare the theoretical predictions with.

The purpose of the present paper is to compare the performance of various non-adiabatic theories in computing the linewidth of electronic intersubband transitions in single and

double square quantum wells – systems in which high quality experimental data exist^{17–23}. Our goal is to clarify the limits of validity of the different approaches, i.e. the ones by Gross and Kohn⁴ and by VUC (the latter is equivalent to the method by Dobson *et al.*¹¹ in the situation considered here). For instance, the formalism of VUC is expected to be exact in the limit of slowly varying density (see above), and in particular does satisfy the HPT. However, this does not necessarily mean that it is the best method under *all* conditions: it will turn out in this paper that the VUC method works well only for those situations where the electronic motion is sufficiently collective. If, on the other hand, a single-particle-like behavior prevails (characterized by large gradients in the velocity field), then the method of Gross and Kohn⁴ gives results which appear to be in better agreement with experiments.

The paper is organized as follows: In Sec. II we introduce the single and double quantum wells used in our comparative studies and calculate their electronic ground state. Sec. III contains a summary of the linear response formalism and the various approximations for the linearized xc potential. In Sec. IV we then calculate the lowest collective intersubband transitions for the single and double quantum wells and compare the results to experiment. Conclusions are given in Sec. V.

II. ELECTRONIC GROUND STATE OF SINGLE AND DOUBLE SQUARE QUANTUM WELLS

Before discussing the linear response in quantum wells, we need to find their electronic ground state. This problem has been dealt with by several authors before^{13,15,19,22,26}, and we give here a summary of the standard procedure to keep this paper self-contained.

We work in the constant effective-mass approximation, taking a value of $m^* = 0.07m$ for the effective electron mass in GaAlAs. We furthermore employ a value of 13.0 for the dielectric constant ϵ , so that the electronic charge becomes $e^* = e/\sqrt{\epsilon}$. In the following, we choose units such that $e^* = m^* = \hbar = 1$. This means that lengths are measured in units of $1 a_0^* = 98.3 \text{ \AA}$, and energies in units of $1 \text{ Hartree}^* = 11.27 \text{ meV}$. The difference between the lower conduction band edges of GaAs and $\text{Al}_{0.3}\text{Ga}_{0.7}\text{As}$ will be taken as 250 meV .

We assume that the quantum wells have been grown along the z -direction and are translationally invariant in the $x - y$ plane. The Kohn-Sham eigenfunctions for an area A are then discrete in the z direction and plane wave-like (with wavevector \mathbf{q}_{\parallel}) perpendicular to it. They can be written as

$$\psi_{\mathbf{q}_{\parallel},j}(\mathbf{r}) = \frac{1}{\sqrt{A}} e^{i\mathbf{q}_{\parallel}\mathbf{r}_{\parallel}} \varphi_j(z), \quad (1)$$

with the Kohn-Sham eigenvalue

$$E(q_{\parallel},j) = \frac{q_{\parallel}^2}{2} + \varepsilon_j. \quad (2)$$

The orbitals $\varphi_j(z)$ satisfy the following Kohn-Sham equation:

$$\left(-\frac{1}{2} \frac{d^2}{dz^2} + v_{\text{ext}}(z) + v_{\text{H}}(z) + v_{\text{xc}}(z) \right) \varphi_j(z) = \varepsilon_j \varphi_j(z). \quad (3)$$

Here, the external potential $v_{\text{ext}}(z)$ is prescribed by the design of the quantum well. For the xc potential $v_{\text{xc}}(z)$ we use the LDA of Vosko, Wilk and Nusair²⁷. The Hartree potential is obtained by direct integration of Poisson's equation as²²

$$v_{\text{H}}(z) = -4\pi \int_{-\infty}^z dz' \int_{-\infty}^{z'} dz'' n_0(z'') + 2\pi N_s z. \quad (4)$$

The sheet density N_s is assumed to be a given constant (typically around 10^{11} cm^{-2}). To determine the density profile in z -direction, $n_0(z)$, we write

$$\begin{aligned} n_0(z) &= 2 \sum_{q_{||}, j} \varphi_j^2(z) \theta(\varepsilon_F - E(q_{||}, j)) \\ &= \frac{1}{2\pi} \sum_{\substack{j \\ \varepsilon_j < \varepsilon_F}} \varphi_j^2(z) (q_F^2 - 2\varepsilon_j), \end{aligned} \quad (5)$$

where ε_F and q_F are the Fermi energy and momentum. The sheet density may thus be expressed as

$$N_s = \int dz n_0(z) = \frac{1}{2\pi} \left(q_F^2 N_{\text{occ}} - 2 \sum_j^{N_{\text{occ}}} \varepsilon_j \right), \quad (6)$$

where N_{occ} indicates the number of occupied orbitals, and the orbitals themselves are assumed to be normalized to one. To close the self-consistency cycle, we now have to determine N_{occ} . To do this, we solve Equation (6) for q_F^2 :

$$q_F^2 = \frac{2\pi}{N_{\text{occ}}} N_s + \frac{2}{N_{\text{occ}}} \sum_j^{N_{\text{occ}}} \varepsilon_j. \quad (7)$$

We now start with $N_{\text{occ}} = 1$ and, if necessary, keep increasing N_{occ} until the condition

$$\varepsilon_{N_{\text{occ}}} < \frac{q_F^2}{2} < \varepsilon_{N_{\text{occ}}+1} \quad (8)$$

is satisfied. In the cases we are interested in (see below), only the lowest subband is occupied, i.e. $N_{\text{occ}} = 1$.

Let us now discuss specific examples of a single and a double square quantum well, both of which have been experimentally studied. The single GaAs square well^{17,18} is taken to have a width of 384 \AA . Note that this value is still within the $\pm 4\%$ range around the design-width 400 \AA of the sample used in the experiments¹⁸. The well is filled with electrons up to a sheet density of $N_s = 0.97 \times 10^{11} \text{ cm}^{-2}$. In the following, we consider only the case of zero gate voltage and neglect any built-in static electric fields.

The (asymmetric) double quantum well¹⁹⁻²³ consists of two GaAs wells of widths 85 \AA and 73 \AA , separated by a 23 \AA barrier of $\text{Al}_{0.3}\text{Ga}_{0.7}\text{As}$. Its electronic sheet density is $N_s = 2 \times 10^{11} \text{ cm}^{-2}$. Again, we consider only the case of zero electric field across the sample.

We have solved the Kohn-Sham equation (3) for the two systems within the LDA. For our choices of N_s , in both cases only the lowest level is occupied in the ground state. The

distribution of the bound levels is illustrated in Figure 1, which also indicates the total effective Kohn-Sham potential of the systems. The energy scale is chosen such that the Fermi level lies at zero. We see that the single square well supports nine bound levels whose spacing grows with increasing energy. The lowest subband spacing is obtained as $E_{12} = 8.18$ meV. The double well, on the other hand, is found to have only four bound levels. Here, the subband spacings are $E_{12} = 11.7$ meV, $E_{13} = 109.2$ meV and $E_{14} = 154.5$ meV.

In the following, we take the ground state of these systems and search for the lowest collective intersubband transition using linear response theory.

III. LINEAR RESPONSE FORMALISM FOR QUANTUM WELLS

A. Response equation

The linear density response within TDDFT is given by

$$n_1(\mathbf{r}, \omega) = \int d^3r' \chi_{\text{KS}}(\mathbf{r}, \mathbf{r}', \omega) v_{\text{eff}}(\mathbf{r}', \omega), \quad (9)$$

where $\chi_{\text{KS}}(\mathbf{r}, \mathbf{r}', \omega)$ is the noninteracting density-density response function, which in our case reads

$$\chi_{\text{KS}}(\mathbf{r}, \mathbf{r}', \omega) = 2 \sum_{\substack{\mu\nu \\ \mathbf{k}_{\parallel}, \mathbf{k}'_{\parallel}}}^{\infty} (f_{\mu} - f_{\nu}) \frac{\psi_{\mathbf{k}_{\parallel}, \mu}(\mathbf{r}) \psi_{\mathbf{k}'_{\parallel}, \nu}^*(\mathbf{r}) \psi_{\mathbf{k}_{\parallel}, \mu}^*(\mathbf{r}') \psi_{\mathbf{k}'_{\parallel}, \nu}(\mathbf{r}')}{\omega - [E(k_{\parallel}, \mu) - E(k'_{\parallel}, \nu)] + i\eta}, \quad (10)$$

with the usual Fermi occupation factors f_{μ} and f_{ν} , and

$$v_{\text{eff}}(\mathbf{r}, \omega) = v_{\text{ext},1}(\mathbf{r}, \omega) + v_{\text{H},1}(\mathbf{r}, \omega) + v_{\text{xc},1}(\mathbf{r}, \omega). \quad (11)$$

Here, $v_{\text{ext},1}(\mathbf{r}, \omega)$ is the frequency-dependent external perturbation, and $v_{\text{H},1}(\mathbf{r}, \omega)$ and $v_{\text{xc},1}(\mathbf{r}, \omega)$ are the linearized Hartree and xc potential. Since our quantum wells are translationally invariant in the $x - y$ plane, we define

$$n_1(\mathbf{q}_{\parallel}, z, \omega) = \int d^2r_{\parallel} e^{-i\mathbf{q}_{\parallel}\mathbf{r}_{\parallel}} n_1(\mathbf{r}, \omega), \quad (12)$$

so that the response equation (9) may be transformed into

$$n_1(\mathbf{q}_{\parallel}, z, \omega) = \int dz' \chi_{\text{KS}}(\mathbf{q}_{\parallel}, z, z', \omega) v_{\text{eff}}(\mathbf{q}_{\parallel}, z', \omega). \quad (13)$$

In the following, we shall only be concerned with the case that $q_{\parallel} = 0$ in Eq. (13). The linearized Hartree potential is then

$$v_{\text{H},1}(z, \omega) = -4\pi \int_{-\infty}^z dz' \int_{-\infty}^{z'} dz'' n_1(z'', \omega). \quad (14)$$

The first-order xc potential will be discussed below.

For the Kohn-Sham response function, we follow Refs. 26,28 and obtain

$$\chi_{\text{KS}}(\mathbf{q}_{\parallel}, z, z', \omega) = \sum_{\mu=1}^{N_{\text{occ}}} \sum_{\nu=1}^{\infty} F_{\mu\nu}(q_{\parallel}, \omega) \varphi_{\mu}(z) \varphi_{\mu}(z') \varphi_{\nu}(z) \varphi_{\nu}(z'), \quad (15)$$

with the definition

$$F_{\mu\nu}(q_{\parallel}, \omega) = \frac{-2}{(2\pi)^2} \int d^2 k_{\parallel} \left\{ \frac{f(\varepsilon_{\mu} + k_{\parallel}^2/2)}{\mathbf{q}_{\parallel} \mathbf{k}_{\parallel} + a_{\mu\nu}(q_{\parallel}) + \omega + i\eta} + \frac{f(\varepsilon_{\mu} + k_{\parallel}^2/2)}{\mathbf{q}_{\parallel} \mathbf{k}_{\parallel} + a_{\mu\nu}(q_{\parallel}) - \omega - i\eta} \right\} \quad (16)$$

and

$$a_{\mu\nu}(q_{\parallel}) = \frac{q_{\parallel}^2}{2} - (\varepsilon_{\mu} - \varepsilon_{\nu}). \quad (17)$$

Setting $q_{\parallel} = 0$ in Eqs. (16) and (17) and performing the integration over k_{\parallel} , we end up with

$$F_{\mu\nu}(q_{\parallel} = 0, \omega) = -\frac{\varepsilon_F - \varepsilon_{\mu}}{\pi} \left\{ \frac{1}{\varepsilon_{\nu} - \varepsilon_{\mu} + \omega + i\eta} + \frac{1}{\varepsilon_{\nu} - \varepsilon_{\mu} - \omega - i\eta} \right\}. \quad (18)$$

This, together with Eq. (15), defines the response function $\chi_{\text{KS}}(\mathbf{q}_{\parallel} = 0, z, z', \omega)$. In the following, we will evaluate χ_{KS} summing only over the *bound* states φ_{ν} , i.e. the ones shown in Figure 1. This approximation is justified by the fact that the collective excitations we are studying are well below the continuum threshold for the quantum wells under consideration and thus involve only the lowest-lying states.

B. Approximations for the xc potential

In our case, the general expression for $v_{\text{xc},1}$ depends only on the z coordinate, and is given by

$$v_{\text{xc},1}(z, \omega) = \int dz' f_{\text{xc}}(z, z', \omega) n_1(z', \omega), \quad (19)$$

where the xc kernel $f_{\text{xc}}(z, z', \omega)$ is a functional of the ground-state density $n_0(z)$.

The simplest possible approximation for $v_{\text{xc},1}$ is the ALDA, which assumes

$$f_{\text{xc}}^{\text{ALDA}}(z, z', \omega) = \delta(z - z') \left. \frac{d^2 e_{\text{xc}}^{\text{hom}}(n)}{dn^2} \right|_{n=n_0(z)}, \quad (20)$$

where $e_{\text{xc}}^{\text{hom}}(n)$ is the xc energy density of the homogeneous electron gas, so that

$$v_{\text{xc},1}^{\text{ALDA}}(z, \omega) = n_1(z, \omega) \left. \frac{d^2 e_{\text{xc}}^{\text{hom}}(n)}{dn^2} \right|_{n=n_0(z)}. \quad (21)$$

In other words, the xc kernel in the ALDA has no frequency dependence at all and is purely real. This approximation is justified for cases where the external potential is slowly varying in time as well as in space.

In a first step towards overcoming the restriction to slow variation in time, Gross and Kohn⁴ proposed the following plausible approximation (which we denote by DLDA, the D standing for “dynamic”), valid for the case where both n_0 and n_1 are slowly varying in space:

$$v_{\text{xc},1}^{\text{DLDA}}(z, \omega) = f_{\text{xc}}^{\text{hom}}(n_0(z), q = 0, \omega) n_1(z, \omega), \quad (22)$$

where $f_{\text{xc}}^{\text{hom}}$ is a property of the homogeneous electron gas, related to the dynamical local field factor as $f_{\text{xc}}^{\text{hom}}(n_0, \omega) = -\lim_{q \rightarrow 0} 4\pi G(q, \omega)/q^2$. Gross *et al.*⁴ have given a simple parametrization of $f_{\text{xc}}^{\text{hom}}(n_0, \omega)$ (see also Ref. 2). A more elaborate calculation of $f_{\text{xc}}^{\text{hom}}(n_0, \omega)$ has recently been performed by Nifosì, Conti and Tosi^{29,30} using an approximate decoupling scheme of the equation of motion for the current density, which accounts for processes of excitation of two electron-hole pairs.

As already discussed in the introduction, the DLDA (22) has recently been found to violate the HPT (for more details see Refs. 8–10). However, a local frequency-dependent approximation which satisfies the HPT can be derived if the current density is taken as basic variable rather than the particle density. The resulting first-order xc vector potential in the form stated by VUC¹⁰ is given by

$$i\omega a_{\text{xc},1,\mu}^{\text{VUC}}(\mathbf{r}, \omega) = \nabla_{\mu} v_{\text{xc},1}^{\text{ALDA}}(\mathbf{r}, \omega) - \frac{1}{n_0(\mathbf{r})} \sum_{\nu} \nabla_{\nu} \sigma_{\text{xc},\mu\nu}(\mathbf{r}, \omega). \quad (23)$$

The dynamical correction to the ALDA xc potential is the divergence of the viscoelastic stress tensor

$$\sigma_{\text{xc},\mu\nu} = \eta_{\text{xc}} \left(\nabla_{\nu} u_{\mu} + \nabla_{\mu} u_{\nu} - \frac{2}{3} \nabla \cdot \mathbf{u} \delta_{\mu\nu} \right) + \zeta_{\text{xc}} \nabla \cdot \mathbf{u} \delta_{\mu\nu}. \quad (24)$$

Here, $\mathbf{u}(\mathbf{r}, \omega) = \mathbf{j}_1(\mathbf{r}, \omega)/n_0(\mathbf{r})$ is the velocity field, and $\eta_{\text{xc}}(\omega, n_0(\mathbf{r}))$ and $\zeta_{\text{xc}}(\omega, n_0(\mathbf{r}))$ are complex viscosity coefficients whose explicit form is given in Ref. 10.

In the one-dimensional case, it is straightforward to derive the associated xc potential⁹. It can be written as

$$v_{\text{xc},1}^{\text{VUC}}(z, \omega) = f_{\text{xc}}^{\text{hom}}(n_0(z), \omega) n_1(z, \omega) - \frac{n'_0(z)}{n_0(z)} f_{\text{xc}}^{\text{dyn}}(z, \omega) \int_{-\infty}^z dz'' n_1(z'', \omega) - \int_z^{\infty} dz' \frac{n'_0(z')}{n_0(z')} f_{\text{xc}}^{\text{dyn}}(z', \omega) n_1(z', \omega) + \int_z^{\infty} dz' \left(\frac{n'_0(z')}{n_0(z')} \right)^2 f_{\text{xc}}^{\text{dyn}}(z', \omega) \int_{-\infty}^{z'} dz'' n_1(z'', \omega). \quad (25)$$

Here, we have defined

$$f_{\text{xc}}^{\text{dyn}}(z, \omega) \equiv f_{\text{xc}}^{\text{hom}}(n_0(z), \omega) - \left. \frac{d^2 e_{\text{xc}}^{\text{hom}}(n)}{dn^2} \right|_{n=n_0(z)}. \quad (26)$$

The first term on the right-hand side of Eq. (25) is the DLDA (22). The other terms are needed to satisfy both the HPT as well as Onsager's reciprocity theorem, i.e. symmetry under interchange of z and z' of the associated xc kernel $f_{\text{xc}}(z, z', \omega)$ (see Ref. 9).

Both the DLDA and the VUC approach lead to a complex xc potential. This means that the frequency of collective modes will come out complex as well, with a negative imaginary part accounting for the damping. As a consequence, care has to be taken to perform

the proper analytic continuation of the Kohn-Sham response function and of f_{xc} , both of which are analytic functions in the upper half complex plane, into the lower half complex plane^{24,31,32}.

The analytic continuation of the response function (15) with (18) is straightforward. This is because there are no branch cuts in the frequency region we consider, and the depolarization shift will move the mode frequency sufficiently far away from the poles in $F_{\mu\nu}(q_{||} = 0, \omega)$. Thus, $\chi_{KS}(q_{||} = 0, z, z', \omega)$ is analytic across the real axis in the frequency region of interest.

For the analytic continuation of f_{xc} , we proceed as shown Ref. 32. The idea is the following: let us assume we have a parametrization of the imaginary part of $f_{xc}(\omega)$ on the real frequency axis. Denote this parametrization by $A_{xc}(\nu)$, where ν is real. Then, the expression for $f_{xc}(\omega)$ in the *upper* complex ω plane is

$$f_{xc}^{up}(\omega) = f_{\infty} + \frac{1}{\pi} \int_{-\infty}^{\infty} \frac{A_{xc}(\nu)}{\nu - \omega} d\nu, \quad \Im\omega > 0. \quad (27)$$

Here, f_{∞} is the large-frequency limit of f_{xc} . The analytic continuation into the *lower* complex ω plane is given by

$$f_{xc}^{lo}(\omega) = f_{\infty} + \frac{1}{\pi} \int_{-\infty}^{\infty} \frac{A_{xc}(\nu)}{\nu - \omega} d\nu + 2iA_{xc}(\omega), \quad \Im\omega < 0. \quad (28)$$

Note that the third term on the right-hand side implies that A_{xc} has to be evaluated at the complex frequency ω , $\Im\omega < 0$. Therefore, in moving down from the real ω axis into the lower half complex plane, one has to make sure along the way that no branch cuts or poles of A_{xc} come across. Due to its simple analytic structure, this is always the case for the parametrization of Gross *et al.*⁴ The expression of Nifosì, Conti and Tosi^{29,30}, however, has to be handled with some caution for large values of $|\Im\omega|$.

C. A simplified approach for the linewidth of collective modes

The linewidth of collective electronic modes can be obtained in a simplified manner^{10,25}. The idea is to first calculate the modes using the ALDA. Outside the regime where Landau damping occurs, the modes will come out undamped, and the mode frequency Ω is purely real. The damping due to dynamical xc effects is then added on perturbatively. For the one-dimensional case, the resulting linewidth (twice the imaginary part of the mode frequency) is given by

$$\Gamma_p = \frac{|\Re \int dz u_1^*(z, \Omega) \frac{\partial}{\partial z} \sigma_{xc,zz}(z, \Omega)|}{\int dz n_0(z) |u_1(z, \Omega)|^2}. \quad (29)$$

From Eq. (23), the derivative of the stress tensor can be written as

$$\frac{\partial}{\partial z} \sigma_{xc,zz}(z, \Omega) = n_0 \frac{\partial}{\partial z} v_{xc,1}^{ALDA}(z, \Omega) - n_0 \frac{\partial}{\partial z} v_{xc,1}(z, \Omega). \quad (30)$$

We therefore obtain the linewidth within the DLDA as

$$\Gamma_p^{\text{DLDA}} = \frac{\int dz \left| \frac{\partial j_1}{\partial z} \right|^2 |\Im f_{\text{xc}}^{\text{hom}}(n_0, \Omega)|}{\Omega \int dz n_0(z) |u_1(z, \Omega)|^2}, \quad (31)$$

and within VUC as

$$\Gamma_p^{\text{VUC}} = \frac{\int dz n_0^2(z) \left| \frac{\partial u_1}{\partial z} \right|^2 |\Im f_{\text{xc}}^{\text{hom}}(n_0, \Omega)|}{\Omega \int dz n_0(z) |u_1(z, \Omega)|^2}. \quad (32)$$

Γ_p^{DLDA} depends on the gradient of the current density j_1 , whereas Γ_p^{VUC} depends on the gradient of the velocity field u_1 . These quantities are related to the density response n_1 via the linearized continuity equation

$$i\Omega n_1 = \frac{\partial j_1}{\partial z} = \frac{\partial}{\partial z} (n_0 u_1). \quad (33)$$

IV. RESULTS AND DISCUSSION

A. Numerical results

Let us now apply the linear response formalism outlined above to the quantum wells whose electronic ground states we have calculated in Section II. The goal is to study the collective intersubband transitions between the first two subbands. Our main interest lies in the damping of these modes.

The standard procedure is to set the external potential $v_{\text{ext},1}$ in the response equation (13) equal to zero. The resulting integral equation for $n_1(z, \omega)$ can then be viewed as a complex eigenvalue problem. The solutions with real eigenvalue 1 are the collective modes of the system. The real part of the mode frequency, $\Omega = \Re\omega$, indicates the position of the mode, and its lifetime is given by $\tau = \Gamma^{-1}$, where $\Gamma = 2\Im\omega$.

Alternatively, one may consider the photoabsorption cross section

$$\sigma(\omega) = \frac{4\pi\omega}{c} \Im\alpha(\omega), \quad (34)$$

where ω is real, and

$$\alpha(\omega) = -\frac{2}{E} \int dz z n_1(z, \omega) \quad (35)$$

is the dipole polarizability associated with an external potential of the form $v_1(z, \omega) = Ez \cos(\omega t)$. We expect to find for our quantum wells that $\sigma(\omega)$ is peaked at the frequency of the collective intersubband transition Ω , with a Lorentzian profile of FWHM Γ .

We have performed both kinds of calculations for the single and double quantum well. In addition, we compare with the linewidths Γ_p following from the simplified approach presented in Sec. III C. Results obtained with the various approaches and approximations are summarized in Tables I and II. The first columns give the mode frequency Ω obtained from ALDA calculations for the collective modes. In both cases, Ω is already quite close

to the experimental result shown in the last column (within 4.2% for the single and within 4.9% for the double square well). However, as mentioned before, the ALDA does not include damping of the modes. This means that $\sigma(\omega)$ would consist of a delta peak at Ω .

The second and third columns in Tables I and II give results for Ω and Γ obtained within the DLDA, using the parametrizations of Gross/Kohn and Nifosì/Conti/Tosi for f_{xc}^{hom} , respectively. Results within the VUC approximation are given in columns four and five, again for the two different parametrizations for f_{xc}^{hom} . The first and third lines show Ω and Γ as obtained from a solution of the response equation for the lowest eigenmode. In the second and fourth line, we show the position and width of the associated peak in the photoabsorption cross section $\sigma(\omega)$. Finally, the last line gives the linewidths Γ_p as obtained from the formulas presented in Sec. III C.

Let us first consider results for the single quantum well, see Table I. We note that for each choice of the xc potential there is an excellent agreement between the results for Ω and Γ computed with the three different methods. The results for Γ_p are extremely close to the linewidths obtained using the full calculation for the collective mode or the photoabsorption cross section, which demonstrates the reliability of the linewidth formulas (31) and (32).

We find that the Gross/Kohn parametrization for f_{xc}^{hom} shifts the mode frequency Ω from its value in ALDA closer towards the experimental value. The agreement is fairly good within the DLDA, but the improvement is only small if the VUC approximation is used. The Nifosì/Conti/Tosi parametrization, on the other hand, leaves the mode frequency Ω practically unchanged, within DLDA as well as VUC.

Compared to the experimental value of 0.53 meV, the linewidth Γ comes out about 25% too high within DLDA, with only small differences between the two parametrizations for f_{xc}^{hom} (0.683 and 0.655 meV, respectively). By contrast, the VUC linewidth is roughly a factor of five smaller than the experimental linewidth. It thus seems as if the DLDA yields a better description of the damping of the modes in the square well.

One has to emphasize, however, that the experimental linewidth contains not only damping effects due to electron-electron interaction, but also caused by additional mechanisms such as finite temperature, scattering off impurities, and fluctuations of the width of the well³³. Therefore, our calculations should provide a strictly lower limit to the measured linewidth. Clearly, this is the case if the VUC approach is used, whereas, under this aspect, the overestimation of the electronic xc damping within the DLDA is substantial. Note that this effect would be even more drastic in a parabolic well: in that case, VUC (which satisfies the HPT) would correctly give zero damping, whereas DLDA would result in an unphysical finite linewidth.

For the double quantum well, however, the situation is different. From Table II, we see that the DLDA results are at least of similar, sometimes even better quality than for the single well. Again, the mode frequency Ω agrees better with experiment if the Gross/Kohn parametrization for f_{xc}^{hom} is used. In that case, the linewidth is slightly smaller than in the experiment (1.00 meV compared to 1.17 meV). With the Nifosì/Conti/Tosi parametrization, it becomes even smaller by almost a factor of three (0.403 meV).

The VUC method, on the other hand, clearly fails to provide an adequate description for the double quantum well. Within the Gross/Kohn parametrization, the mode frequency Ω drastically overshoots the experimental value by about 40%. The opposite happens with the Nifosì/Conti/Tosi parametrization, which shifts the ALDA value for Ω down by more

than 1 meV. In both cases, the linewidth is dramatically too high. We also observe some differences between the results obtained from calculating the complex mode frequency and the photoabsorption cross section. Moreover, the linewidth formulas (31) and (32) seem to break down here. This obvious failure of the VUC method for the double well calls for some explanation. We shall therefore examine the nature of the electron dynamics in the two quantum wells more closely.

B. Physical picture: collective vs. single-particle

To get some feeling for the underlying physics of the dynamical processes involved, it is helpful to look directly at the local behavior of various quantities characterizing the response of the electron liquid.

Fig. 2 shows the ground-state density $n_0(z)$ for the single square well and the density profile of its lowest collective mode, $n_1(z)$, together with the current density $j_1(z)$ and the velocity field $u_1(z)$. Calculations have been done within the ALDA. The other approximations for the xc potential give very similar results. All quantities plotted in Fig. 2 vary quite smoothly across the well. Note that for the case of a parabolic well, $n_0(z)$ and $j_1(z)$ would have an identical shape, so that the velocity field $u_1(z)$ would be uniform. Here, however, $u_1(z)$ has a shape similar to (though slightly smoother than) that of $n_0(z)$ and $j_1(z)$, which may be viewed as an illustration for the non-parabolicity of the square well.

The same quantities have been plotted for the double quantum well in Fig. 3. Here, the ground-state density $n_0(z)$ has two peaks, the lower one at the narrower well and the higher one at the wider well. The dip in $n_0(z)$ is at the position of the barrier between the two wells. The density response $n_1(z)$ does not deviate too much from the one found for the single well, see Fig. 2, apart for a slight hump at the barrier. The strongest differences, however, show up in the current density and the velocity field. We see from Fig. 3 that $j_1(z)$ is very smoothly varying across the system, apparently ignoring the presence of the barrier between the wells. The velocity field $u_1(z)$, however, is strongly peaked at the position of the barrier.

From the examples shown in Figs. 2 and 3, we see that the most sensitive indicator for the physical nature, or rather the degree of “collectiveness”, of the motion of the electron liquid is the velocity field $u_1(z)$. Two extreme cases have to be distinguished: (i) Collective motion, as realized in a perfect way in a parabolic well. The velocity field is then only slowly varying. This is the case on which the HPT is based. (ii) Single-particle-like motion, occurring for instance in a tunneling process through a classically forbidden region, like the barrier between the two wells. Such a process is characterized by a pronounced peak in the velocity field, or, more generally speaking, by the presence of large gradients in $u_1(z)$. We are thus led to consider more closely the gradients of the various quantities involved.

Note that the domain of validity for the VUC method is restricted by the conditions^{8–10} $k \ll \omega/v_F, k_F$ and $q \ll \omega/v_F, k_F$, where k^{-1} and q^{-1} are the characteristic length scales for variation of the external potential and equilibrium density, respectively, and k_F and v_F are the local Fermi momentum and velocity. For the problems considered here (calculation of the photoabsorption cross section), the variation of the external potential is negligible, i.e. the condition on k is fulfilled. In turn, a measure for q is given by the quantity $|n'_0(z)|/n_0(z)$.

The top parts of Figs. 4 and 5 compare the local values of k_F and ω/v_F with $|n'_0|/n_0$ for the single and double well. For the single well, the condition $|n'_0|/n_0 < \omega/v_F, k_F$ is reasonably well satisfied for the central part of the density distribution, but not towards the borders of the potential well. Note that a similar behavior would be found for a parabolic well. For the double well in Fig. 5, by contrast, the same condition is much more strongly violated, due to the fact that there are large density gradients around the region of the potential barrier in the middle.

From the definition of the velocity (see Eq. (33)), we can write

$$\frac{n'_0(z)}{n_0(z)} = \frac{j'_1(z)}{j_1(z)} - \frac{u'_1(z)}{u_1(z)}. \quad (36)$$

The two quantities on the right-hand side are plotted in the lower parts of Figs. 4 and 5, again comparing with the local k_F . We see that for the single quantum well, $|u'_1|/u_1$ lies consistently below $|j'_1|/j_1$. For the double well, however, the situation is opposite: $|u'_1|/u_1$ has sharp structures around the position of the barrier and is much greater than k_F , whereas $|j'_1|/j_1$ is relatively smooth over the whole interior of the system. Note, finally, that for the case of a parabolic quantum well we would have $n'_0/n_0 = j'_1/j_1$ since here the velocity gradient vanishes.

We thus see immediately from Eqs. (31) and (32) that $\Gamma^{\text{VUC}} \gg \Gamma^{\text{DLDA}}$ for the double well is explained by the large values of $|u'_1|/u_1$. This suggests an additional, more refined local criterion for applicability of the VUC approach, requiring that $|\nabla \mathbf{u}_1(\mathbf{r})|/u_1(\mathbf{r}) \ll |\nabla \mathbf{j}_1(\mathbf{r})|/j_1(\mathbf{r})$. This condition is closely related to the hydrodynamical picture inherent in VUC. It may be viewed as requiring a high degree of collectivity of the motion of the electron liquid in the system. This also suggests a pragmatic way to deal with the question of which method to choose for approximating the dynamic xc potential for an arbitrary system: use VUC only in those regions of space where the electronic motion is predominantly collective, i.e. where $|\nabla \mathbf{u}_1(\mathbf{r})|/u_1(\mathbf{r}) < |\nabla \mathbf{j}_1(\mathbf{r})|/j_1(\mathbf{r})$. In those regions where the velocity gradients are large (i.e. the motion is more single-particle like), use the much more robust DLDA. Note that this prescription automatically satisfies the HPT. The so defined VUC-DLDA hybrid scheme yields a linewidth which always lies below the linewidths of the two “pure” schemes, or at most equals the smaller one.

We have applied the VUC-DLDA hybrid scheme to our quantum wells. From Fig. 4 it can be seen that for the single well the VUC-DLDA scheme coincides with the VUC method since here the velocity field is always smoother than the current density. In contrast, Fig. 5 for the double well shows that within VUC-DLDA the central part is treated with the DLDA, whereas the VUC is used for the outer region. Numerical results are shown in Table III. Compared to DLDA (see Table II), the resulting mode frequency Ω is somewhat smaller if the Gross-Kohn parametrization is used, and almost unchanged with the Nifosì/Conti/Tosi parametrization. The effect on the linewidth is more pronounced: for both parametrizations, it is reduced to roughly half of its DLDA value, and is now substantially smaller than the experimental value, as it should.

Fig. 6 illustrates the transition between the “collective” and the “single-particle-like” regime. We calculate the linewidth and lowest collective mode frequency (using ALDA and the linewidth formulas of Sec. III C) for our asymmetric double quantum well with variable barrier height, from its maximum value used so far, down to zero (which then

defines a single square well of width 181\AA). All the while, the electronic sheet density is kept constant. The calculations have been done using the Gross/Kohn parametrization (the other parametrization yields similar results). We see that for decreasing barrier height, the VUC linewidth shrinks much more rapidly than the DLDA linewidth. The crossover occurs around 0.3 times the maximum height. This is the region where the mode frequency becomes comparable to the barrier height. The VUC-DLDA results, on the other hand, lie consistently below the DLDA results, and merge with VUC for small barrier heights, indicating a high degree of collectivity.

V. CONCLUSION

In this work, we have carried out a comparative study of two approaches to describe the linear electronic response of quantum wells within a density-functional framework. The two methods are the dynamical extension of the ALDA by Gross and Kohn (DLDA) and the recent implementation of time-dependent current density functional theory describing dynamical exchange and correlation in the language of conventional hydrodynamics (VUC). The latter approach is rigorously justified in the limit of slowly varying density, in the sense that it satisfies the harmonic potential theorem and other exact Ward identities and symmetries, which in turn are violated by the DLDA. A third approach, recently proposed by Dobson, Büchner and Gross¹¹, turns out to coincide with VUC in the case of one-dimensional inhomogeneity studied here.

Our studies show that the VUC functional should be applied in general only with a certain caveat, since there are physical situations of interest where it fails to work. Its domain of applicability was found to be closely linked to the structure of the velocity field of the electronic motion. If the latter is sufficiently smooth - which indicates a high degree of collective motion - then VUC leads to sensible results. On the other hand, if there are large gradients of the velocity field (as observed around the nonclassical barrier region in the double well), then VUC is obviously inadequate. By contrast, the DLDA approach was found to be much less sensitive to the nature of the electronic motion and led to a reasonably good description of the double well, although it clearly overdamps the predominantly collective motion in the single well.

We finally proposed a pragmatic answer to the question of which functional to choose in a general case. We introduced a hybrid scheme using either VUC or DLDA in their respective spatial region of applicability. This provides a robust method to describe damping of electronic modes of either collective or single-particle-like nature, as shown for the case of a double well with variable barrier height.

ACKNOWLEDGMENTS

This work was supported by Research Board Grant RB 96-071 from the University of Missouri and by NSF grant No. DMR-9706788. We thank Sergio Conti and Jon Williams for useful discussions.

REFERENCES

- ¹ E. Runge and E. K. U. Gross, Phys. Rev. Lett. **52**, 887 (1984).
- ² E. K. U. Gross, J. F. Dobson, and M. Petersilka, in *Density Functional Theory II*, edited by R. F. Nalewajski, Topics in Current Chemistry Vol. 181 (Springer, Berlin, 1996).
- ³ A. Zangwill and P. Soven, Phys. Rev. Lett. **45**, 204 (1980); Phys. Rev. B **24**, 4121 (1981).
- ⁴ E. K. U. Gross and W. Kohn, Phys. Rev. Lett. **55**, 2850 (1985); erratum ibid. **57**, 923 (1986); N. Iwamoto and E. K. U. Gross, Phys. Rev. B **35**, 3003 (1987).
- ⁵ J. Dobson, Phys. Rev. Lett. **73**, 2244 (1994).
- ⁶ G. Vignale, Phys. Rev. Lett. **74**, 3233 (1995).
- ⁷ W. Kohn, Phys. Rev. **123**, 1242 (1961); L. Brey, N. F. Johnson, and B. I. Halperin, Phys. Rev. B **40**, 10647 (1989); L. Brey, J. Dempsey, N. F. Johnson, and B. I. Halperin, Phys. Rev. B **42**, 1240 (1990); S. K. Yip, Phys. Rev. B **43**, 1707 (1991).
- ⁸ G. Vignale and W. Kohn, Phys. Rev. Lett. **77**, 2037 (1996).
- ⁹ G. Vignale and W. Kohn, in *Electronic Density Functional Theory*, edited by J. Dobson, M. K. Das, and G. Vignale (Plenum Press, New York, 1996).
- ¹⁰ G. Vignale, C. A. Ullrich, and S. Conti, Phys. Rev. Lett. **79**, 4878 (1997).
- ¹¹ J. F. Dobson, M. J. Büchner, and E. K. U. Gross, Phys. Rev. Lett. **79**, 1905 (1997).
- ¹² P. R. Pinsukanjana, E. G. Gwinn, J. F. Dobson, E. L. Yuh, N. G. Asmar, M. Sundaram, and A. C. Gossard, Phys. Rev. B **46**, 7284 (1992).
- ¹³ J. F. Dobson, Phys. Rev. B **46**, 10163 (1992).
- ¹⁴ A. Wixforth, M. Kaloudis, C. Rocke, K. Ensslin, M. Sundaram, J. H. English, and A. C. Gossard, Semicond. Sci. Technol. **9**, 215 (1994).
- ¹⁵ N. G. Asmar and E. G. Gwinn, Phys. Rev. B **46**, 4752 (1992).
- ¹⁶ E. L. Yuh, E. G. Gwinn, P. R. Pinsukanjana, W. L. Schaich, K. L. Campman, P. F. Hopkins, and A. C. Gossard, Phys. Rev. B **54**, 11467 (1996).
- ¹⁷ K. Craig, C. L. Felix, J. N. Heyman, A. G. Markelz, M. S. Sherwin, K. L. Campman, P. F. Hopkins, and A. C. Gossard, Semicond. Sci. Technol. **9**, 627 (1994).
- ¹⁸ K. Craig, Ph.D. thesis, University of California, Santa Barbara, 1997 (unpublished).
- ¹⁹ J. N. Heyman, K. Craig, B. Galdrikian, M. S. Sherwin, K. Campman, P. F. Hopkins, S. Fafard, and A. C. Gossard, Phys. Rev. Lett. **72**, 2183 (1994).
- ²⁰ J. N. Heyman, K. Unterrainer, K. Craig, B. Galdrikian, M. S. Sherwin, K. Campman, P. F. Hopkins, and A. C. Gossard, Phys. Rev. Lett. **74**, 2682 (1995).
- ²¹ M. S. Sherwin, K. Craig, B. Galdrikian, J. Heyman, A. Markelz, K. Campman, S. Fafard, P. F. Hopkins, and A. Gossard, Physica D **83**, 229 (1995).
- ²² B. Galdrikian and B. Birnir, Phys. Rev. Lett. **76**, 3308 (1996).
- ²³ J. B. Williams, K. Craig, M. S. Sherwin, K. Campman, and A. C. Gossard, to be published.
- ²⁴ D. Pines and P. Nozières, *The Theory of Quantum Liquids* (W. A. Benjamin, New York, 1966).
- ²⁵ C. A. Ullrich and G. Vignale, to be published.
- ²⁶ J. F. Dobson, in *Density Functional Theory*, Vol. 337 of *NATO ASI Series B*, ed. by E. K. U. Gross and R. M. Dreizler (Plenum Press, New York, 1995), p. 393.
- ²⁷ R. M. Dreizler and E. K. U. Gross, *Density Functional Theory: An Approach to the Quantum Many-Body Problem* (Springer-Verlag, Berlin, 1990).
- ²⁸ A. G. Eguluz, Phys. Rev. B **31**, 3303 (1985)

- ²⁹ H. M. Böhm, S. Conti, and M. P. Tosi, *J. Phys.: Condens. Matter* **8**, 781 (1996); S. Conti, R. Nifosì, and M. P. Tosi, *J. Phys.: Condens. Matter* **9**, L475 (1997).
- ³⁰ R. Nifosì, S. Conti, and M. P. Tosi, to be published.
- ³¹ J. F. Dobson and G. H. Harris, *J. Phys. C: Solid State Phys.* **21**, L729 (1988).
- ³² J. F. Dobson, G. H. Harris, and A. J. O'Connor, *J. Phys. Condens. Matter* **2**, 6461 (1990).
- ³³ To estimate the contribution of the last effect to the line broadening, note that changing the width of the well by one monolayer (about 3\AA) shifts the real part of the mode frequency by about 0.1 meV.

FIGURES

FIG. 1. Full lines: effective Kohn-Sham potential along the growth direction for the electronic ground state of the single and double square wells. The electronic sheet densities are $0.97 \times 10^{11} \text{ cm}^{-2}$ and $2 \times 10^{11} \text{ cm}^{-2}$, respectively. The dashed lines indicate the bound single-particle levels. The energy scale is such that the Fermi energy lies at zero. Only the lowest level is occupied in both cases. The collective transitions we are interested in take place between the two lowest subbands.

FIG. 2. Top: ground-state density profile $n_0(z)$ for the single square well, see Fig. 1. Middle: density profile $n_1(z)$ of the lowest collective mode, calculated within the ALDA. Bottom: associated current density $j_1(z)$ and velocity profile $u_1(z)$. The latter has been scaled with a factor of 0.05.

FIG. 3. Same as Fig. 2, for the double quantum well.

FIG. 4. Top: rate of variation of the ground-state density, $|n'_0(z)|/n_0(z)$, of the single square well, versus local k_F and ω/v_F . Bottom: rate of variation of associated current density j_1 and velocity profile u_1 .

FIG. 5. Same as Fig. 4, for the double quantum well.

FIG. 6. Ratio of linewidth Γ_p and lowest collective mode frequency Ω for the double well with barrier height varying from zero to one, where one corresponds to the full height. Calculations are done with ALDA and the linewidth formulas of Sec. III C, using the VUC, DLDA and VUC-DLDA hybrid scheme, as indicated.

TABLES

TABLE I. Lowest collective intersubband transition of the single GaAs/AlGaAs square well, calculated with various approaches for the linearized xc potential. The superscript 1 (2) stands for the parametrization by Gross/Kohn (Nifosì/Conti/Tosi) for f_{xc}^{hom} . Ω is the frequency of the mode, Γ its width. The subscripts indicate the computational scheme: search for the eigenmode of the system as pole in the complex ω -plane (m), calculation of the photoabsorption cross section (σ), and using the simplified approach from Sec. III C (p). All numbers are given in meV.

	ALDA	DLDA ¹	DLDA ²	VUC ¹	VUC ²	Exp.
Ω_m	10.25	10.63	10.23	10.31	10.24	10.7
Ω_σ		10.63	10.24	10.31	10.24	
Γ_m		0.683	0.655	0.128	0.104	0.53
Γ_σ		0.683	0.639	0.128	0.104	
Γ_p		0.686	0.636	0.130	0.104	

TABLE II. Same as Table I, for the double square well.

	ALDA	DLDA ¹	DLDA ²	VUC ¹	VUC ²	Exp.
Ω_m	13.85	14.24	13.88	20.64	12.55	14.6
Ω_σ		14.24	13.89	20.23	12.89	
Γ_m		1.00	0.403	8.55	4.15	1.17
Γ_σ		1.00	0.401	8.52	3.52	
Γ_p		0.988	0.406	11.07	6.50	

TABLE III. Same as Table II, for the double square well, using the VUC-DLDA scheme.

	VUC-DLDA ¹	VUC-DLDA ²	Exp.
Ω_m	14.07	13.87	14.6
Γ_m	0.620	0.194	1.17
Γ_p	0.605	0.192	

Fig. 1

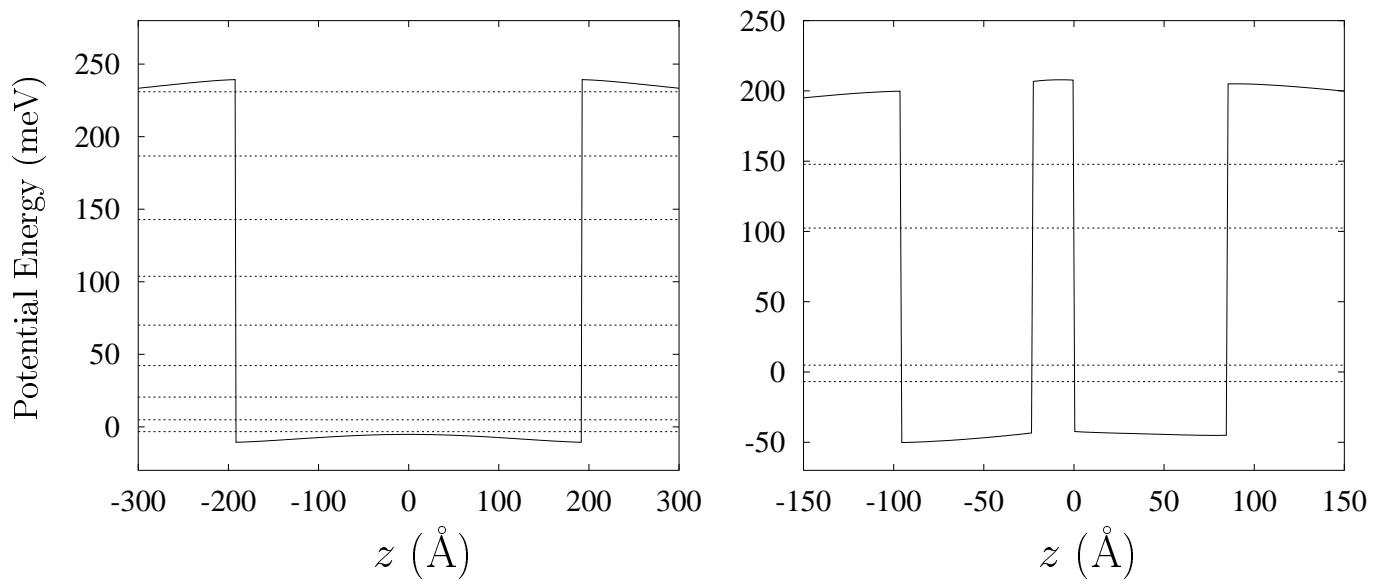


Fig. 2

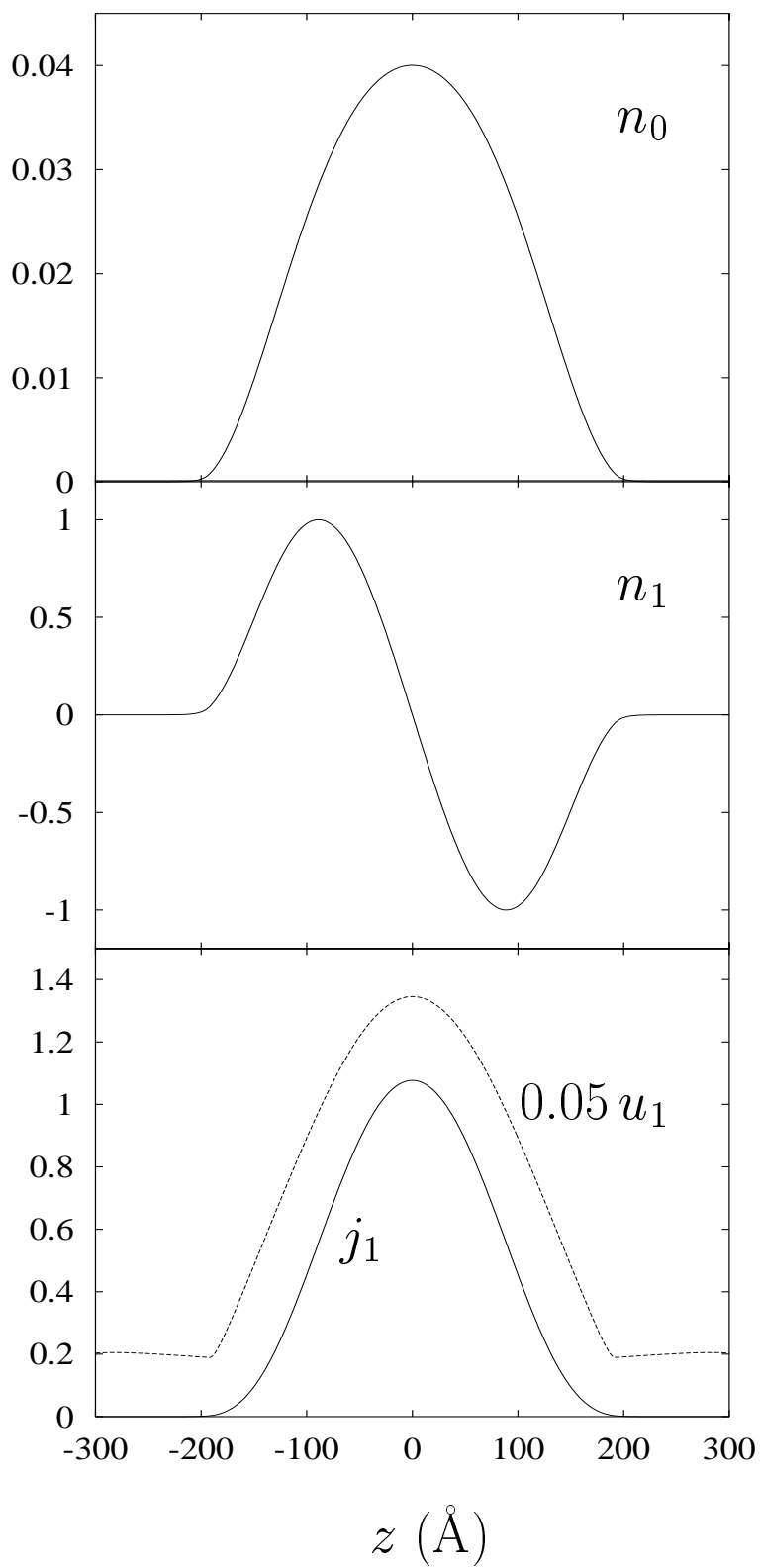


Fig. 3

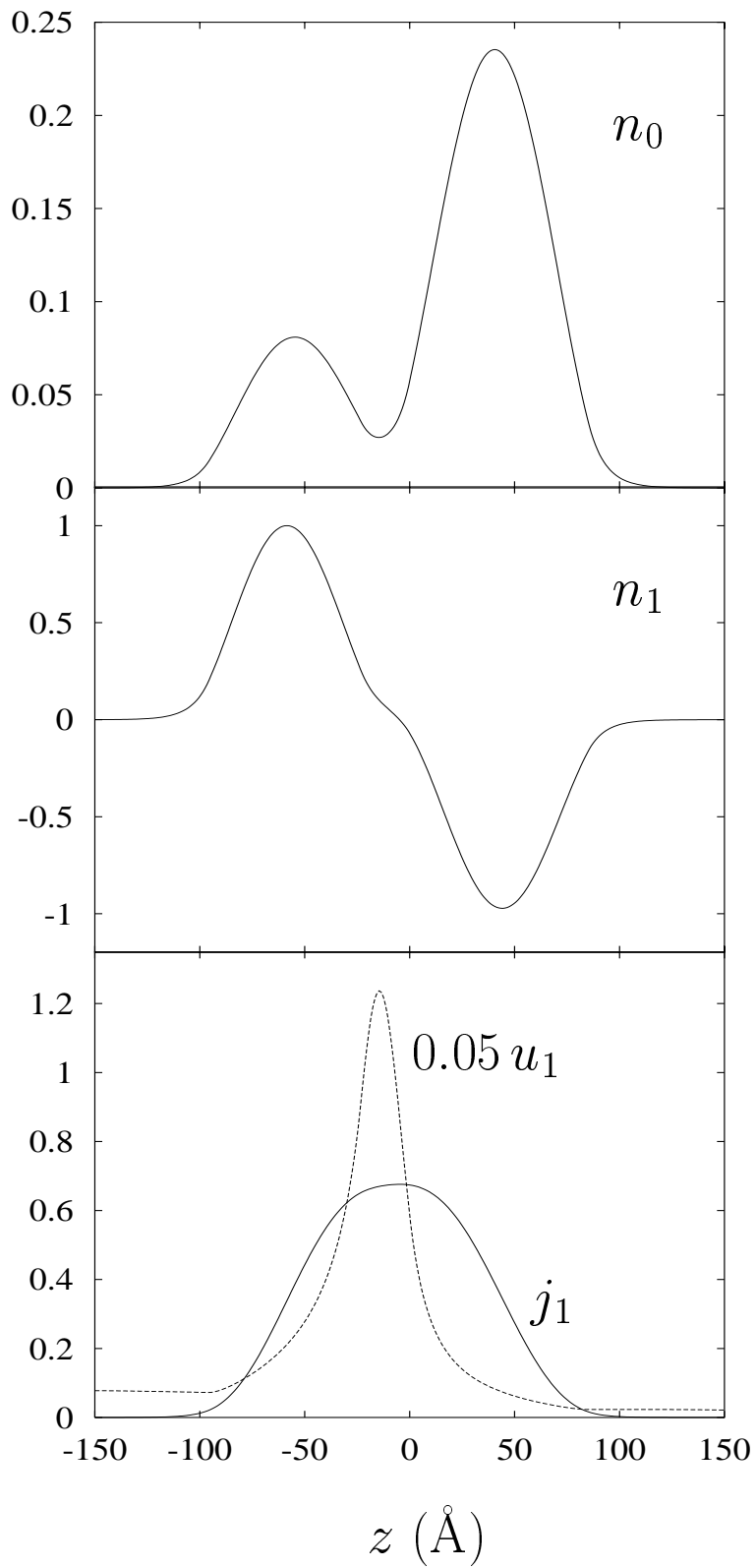


Fig. 4

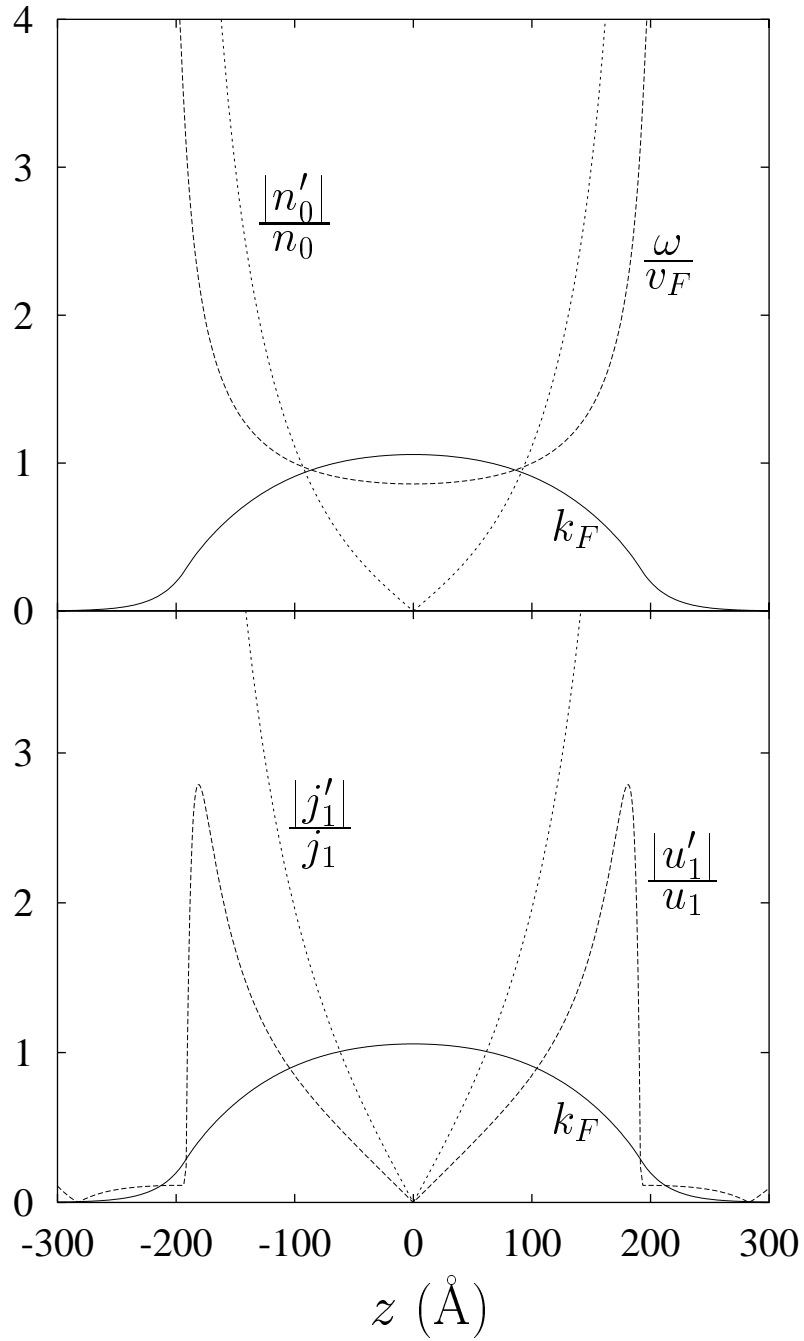


Fig. 5

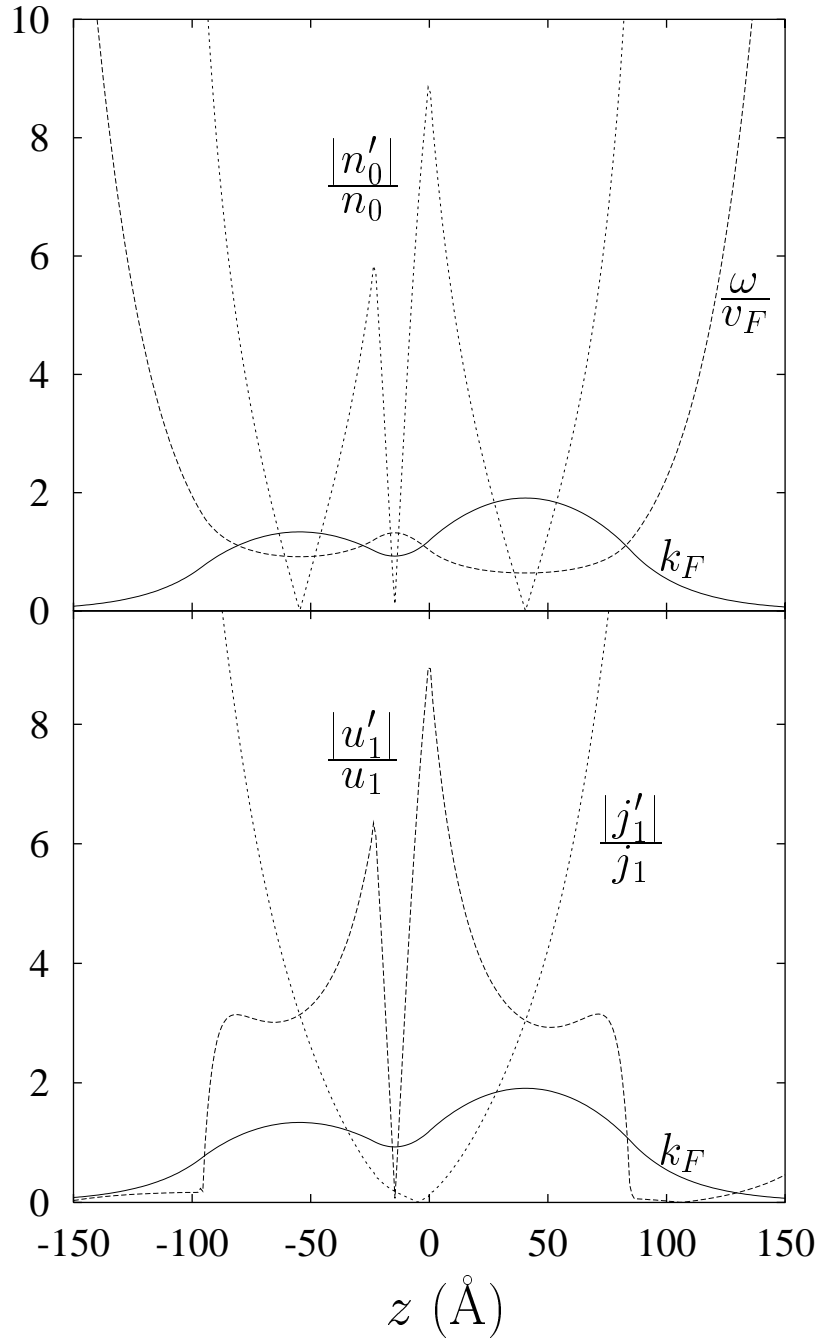


Fig. 6

